

Structural insight into dimeric interaction of the SARAH domains from Mst1 and RASSF family proteins in the apoptosis pathway

Eunha Hwang*, Kyoung-Seok Ryu*, Kimmo Pääkkönen†, Peter Güntert†, Hae-Kap Cheong*, Dae-Sik Lim‡, Jie-Oh Lee§, Young Ho Jeon*¶, and Chaejoon Cheong*¶

*Magnetic Resonance Team, Korea Basic Science Institute, 804-1 Yangchung-Ri, Ochang, Chungbuk 363-883, Korea; †Tatsuo Miyazawa Memorial Program, RIKEN Genomic Sciences Center, 1-7-22 Suehiro-cho, Tsurumi, Yokohama 230-0045, Japan; Departments of ‡Biological Sciences and §Chemistry, Korea Advanced Institute of Science and Technology, 373-1 Guseong-D, Yuseong-G, Daejeon 305-701, Korea

Edited by Alfred G. Redfield, Brandeis University, Waltham, MA, and approved April 16, 2007 (received for review December 5, 2006)

In eukaryotic cells, apoptosis and cell cycle arrest by the Ras → RASSF → MST pathway are controlled by the interaction of SARAH (for Salvador/Rassf/Hippo) domains in the C-terminal part of tumor suppressor proteins. The Mst1 SARAH domain interacts with its homologous domain of Rassf1 and Rassf5 (also known as Nore1) by forming a heterodimer that mediates the apoptosis process. Here, we describe the homodimeric structure of the human Mst1 SARAH domain and its heterotypic interaction with the Rassf5 and Salvador (Sav) SARAH domain. The Mst1 SARAH structure forms a homodimer containing two helices per monomer. An antiparallel arrangement of the long α -helices (h2/h2') provides an elongated binding interface between the two monomers, and the short 3_{10} helices (h1/h1') are folded toward that of the other monomer. Chemical shift perturbation experiments identified an elongated, tight-binding interface with the Rassf5 SARAH domain and a 1:1 heterodimer formation. The linker region between the kinase and the SARAH domain is shown to be disordered in the free protein. These results imply a novel mode of interaction with RASSF family proteins and provide insight into the mechanism of apoptosis control by the SARAH domain.

tumor suppressor | cell cycle arrest | Hippo | Salvador

Recent work in cellular homeostasis has uncovered a pathway mediated by the MST (mammalian sterile 20-like kinase) family, the human ortholog for Hippo (Hpo), which promotes apoptosis and restricts cell proliferation in conjunction with RASSF family tumor suppressors and/or the scaffold protein Salvador (Sav) (1–6). This pathway is characterized by a unique interaction motif called SARAH (for Sav/Rassf/Hpo), which connects the proteins involved in this pathway (7).

Mammalian sterile 20-like kinase 1 (Mst1, also called STK4) is a member of a family of serine/threonine kinases that show similarity to Ste20, an upstream activator of the MAPK pathway in budding yeast (8, 9). Mst1 is cleaved by caspase 3, which is triggered either by the activation of death receptors, such as Fas and the TNF- α receptor, or by exposure of the cells to inducers of apoptosis, such as staurosporine or ceramide (10–13). Whereas intact Mst1 is localized predominantly in the cytoplasm, the catalytic fragment of Mst1 generated by caspase-mediated cleavage translocates to the nucleus and phosphorylates histone H2B at Ser-14, resulting in chromatin condensation, DNA fragmentation, and, ultimately, cell death by apoptosis (14, 15).

A *Drosophila* homolog of Mst1/2, Hippo (Hpo), together with Salvador (Sav) and Warts (Wts), promotes both proper exit from the cell cycle and apoptosis during development (1–3). Mst1 and Mst2 have also been shown to associate with members of the RASSF family of tumor suppressors, such as Rassf1 and Rassf5 (also known as Nore1), all of which contain a conserved Ras-association (RA) domain, with both of the MST and RASSF proteins colocalizing to microtubules throughout the cell cycle (4–6). Whereas purified recombinant Rassf1A inhibited the kinase

activity of purified recombinant Mst1 *in vitro*, overexpression of Rassf1A increased the kinase activity of Mst1 in intact cells, suggesting that the regulation of Mst1 by Rassf1A *in vivo* involves more than the simple association of the two proteins (16).

The C-terminal part of Mst1 contains a protein–protein interaction domain, called SARAH, which spans \approx 50 residues (7). The SARAH domain mediates both homodimerization and heterotypic interaction. MST is autoactivated by autophosphorylation of a threonine residue (Thr-183 of Mst1 and Thr-180 of Mst2). The autoactivation of Mst1 is inhibited by the deletion of the SARAH domain, which implies a role of this homodimerization. On the other hand, the interaction between RASSF and MST mediates MST activation and thereby promotes apoptosis induced by death receptor signaling (16). Thus, the SARAH-mediated homo- and heterodimerization are crucial in the pathways that induce apoptosis and cell cycle arrest.

To investigate the mechanism mediated by the SARAH domain, it is essential to understand how the SARAH domain recognizes its dimerization partners. Currently, there is no structural information on the SARAH domain association. Here, we present the structure of the human Mst1 SARAH homodimer and its interaction with Rassf1 and Rassf5.

Results

SARAH Folds into a Dimeric Antiparallel Helix Structure. We determined the three-dimensional structure of the human Mst1 SARAH domain (residues 432–480) by using heteronuclear NMR spectroscopy. The Mst1 SARAH domain forms a symmetric homodimer in solution. The structure is defined well by the NMR data [Fig. 1 and supporting information (SI) Table 1]. Each monomer consists of two helices (h1, residues 433–437; h2, residues 441–480). The short N-terminal 3_{10} helix h1 is folded toward the corresponding helix h1' of the other monomer. Hydrophobic interactions between helices h1 and h2, involving the side chains of residues 436, 439, 441, and 444 from one monomer and 473 and 477 from the other monomer stabilize the conformation of the N-terminal helix (Fig. 2C). Bifurcated hydrogen bonds where both NH protons of Ser-438 and Trp-439

Author contributions: Y.H.J. and C.C. designed research; E.H., K.-S.R., and Y.H.J. performed research; H.-K.C. and D.-S.L. contributed new reagents/analytic tools; K.-S.R., K.P., P.G., and J.-O.L. analyzed data; and P.G., Y.H.J., and C.C. wrote the paper.

The authors declare no conflict of interest.

This article is a PNAS Direct Submission.

Abbreviation: RDC, residual dipolar coupling.

Data deposition: The atomic coordinates and structure factors have been deposited in the Protein Data Bank, www.pdb.org (PDB ID code 2J08).

¶To whom correspondence may be addressed. E-mail: yhjeon@kbsi.re.kr or cheong@kbsi.re.kr.

This article contains supporting information online at www.pnas.org/cgi/content/full/0610716104/DC1.

© 2007 by The National Academy of Sciences of the USA

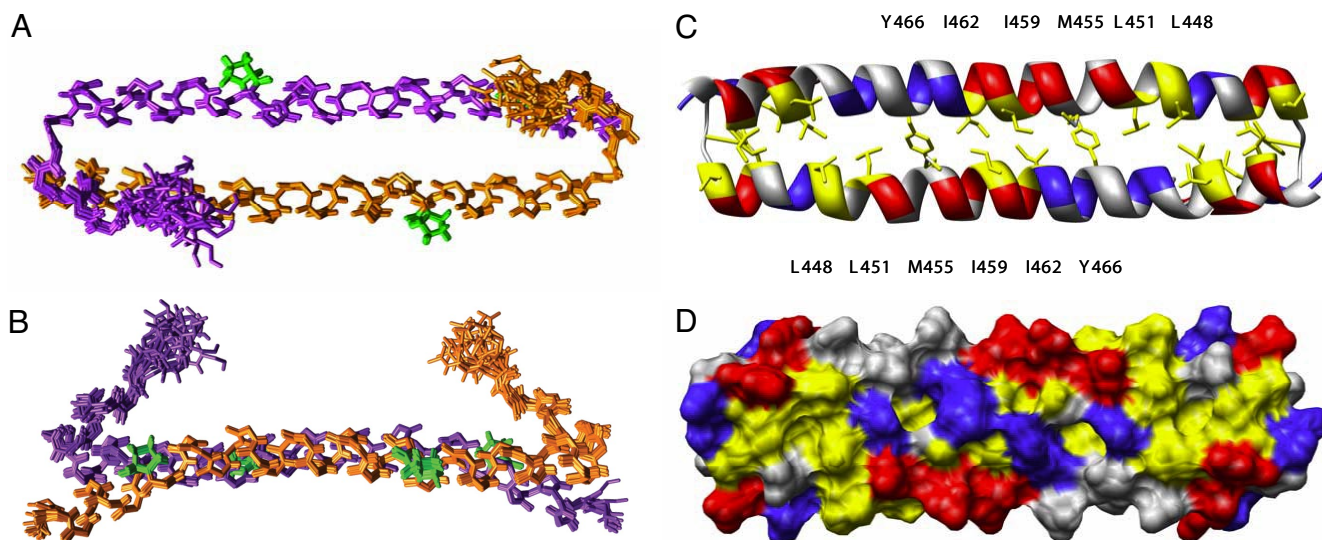


Fig. 1. Solution structure of the human Mst1 SARAH domain (residues 432–480). (A) Ensemble of the 10 lowest-energy NMR conformers of the human Mst1 SARAH dimer. The two monomers are colored magenta and orange, respectively. Proline residues are green. (B) Same structure as in A rotated by 90° around a horizontal axis. (C and D) Ribbon (C) and surface representation (D) of the human Mst1 SARAH dimer in the same orientation as in A. Positively and negatively charged residues are colored blue and red, respectively. Hydrophobic residues are yellow.

are hydrogen bonding to the same CO of Phe-435 additionally stabilize the h1 helix (Fig. 2C). Helix h2 is very elongated and spans 40 residues corresponding to 11 helical turns. Slight distortions occur at the proline residues Pro-453 and Pro-472. The angle between the axes of helices h1 and h2 is $\approx 45^\circ$.

The dimer is formed by a head-to-tail interaction of the two monomers, forming an antiparallel helix dimer between h2 and h2'. The dimer interface is stabilized by hydrophobic interactions, mainly involving aliphatic side chains in helix h2, as evidenced by intermolecular nuclear Overhauser effects (NOEs) for residues Leu-444, Leu-448, Leu-451, Met-455, Ile-459, Ile-462, and Tyr-466 (Fig. 1C). Intermolecular electrostatic interactions between Asp-452 and Arg-470 additionally stabilize the dimer interface. The dimer interface was corroborated by a transferred cross-saturation experiment (17), which showed a >50% reduction of the peak intensities from the residues in the interface upon irradiation (Fig. 2A and B).

The dimeric conformation of the human Mst1 SARAH domain was confirmed by light-scattering measurements, gel filtration chromatography, and cross-linking experiments (see Fig. 4B). The ^1H - ^{15}N heteronuclear NOE shows that the N-terminal h1 helix has a rigidity similar to that of the long h2 helix (Fig. 2D). The ^1H - ^{15}N residual dipolar coupling (RDC) values were used to confirm the degree of bending of the long h2 helix, and the orientation of the h1 helix (Fig. 2D).

Searches in the Protein Data Bank with Dali (18) or MSDfold (19) did not reveal any close structural homologs, indicating that the SARAH dimer represents a novel fold.

Interaction with the SARAH Domains from the RASSF Family. Mst1 and Mst2 have been shown to associate with members of the RASSF family of tumor suppressors, such as Rassf1 and Rassf5, through the interaction of their SARAH domains. We used NMR titration (Fig. 3A–C) and cross-linking (Fig. 4B) experiments to characterize the heterotypic interaction of SARAH domains. We expressed the Rassf1 SARAH domain (residues 220–270) and the Rassf5 SARAH domain (residues 366–413) as GST-fused proteins. Because the purified Rassf1 SARAH domain was not soluble, we conducted the chemical shift perturbation experiment by using the Rassf5 SARAH domain. In cross-linking experiments, the major population of the free

Rassf5 SARAH domain formed tetramers in solution. However, when the Mst1 SARAH domain was added, dimers were formed (Fig. 4B). Addition of purified Rassf5 SARAH domain to ^{15}N -labeled Mst1 SARAH domain induces large changes in ^1H - ^{15}N correlation spectra (Fig. 3A), with signals of the free form disappearing and reappearing at new positions. The slow exchange on the NMR chemical shift time scale between free and bound states is indicative of tight binding with a dissociation constant in the nanomolar range. The titration curve (Fig. 4A) and the line widths in the NMR spectra indicate a 1:1 stoichiometry for the Mst1·Rassf5 complex in solution.

In the chemical shift perturbation experiment, the entire range of the Mst1 SARAH dimer showed signal changes upon the addition of the Rassf5 SARAH domain. It indicates the greatest part of the Mst1 SARAH domain structure involved in the binding with Rassf5. Comparing the cross-saturation data of the homodimer, we find that the Rassf5-binding face of the Mst1 SARAH domain is on the same side of the homodimeric interface at the h2 helix (Fig. 3D). Addition of a molar excess of Rassf5 to the Mst1 SARAH domain induced the appearance of many additional NMR signals in the region of 8.5–9.0 ppm (SI Fig. 6), which implies a further conformational change of the Mst1 SARAH domain upon interaction with Rassf5.

Interaction with the Human Salvador (WW45) SARAH Domain. We performed similar experiments also with human Salvador (Sav, also known as WW45) (20). In NMR binding experiments, addition of the Sav SARAH domain (residues 321–373) to the Mst1 SARAH domain resulted in signal broadening for many residues (Lys-437, Leu-444, Leu-449, Glu-458, Lys-465, Gln-467, Lys-469, Gln-471, Ile-473, Asp-475, Glu-478) of the Mst1 SARAH domain (Fig. 3B and E), indicating that the Sav SARAH domain binds to the Mst1 SARAH domain. However, the addition of the Sav SARAH domain to the Mst1·Rassf5 complex did not change significantly the Mst1 signals (Fig. 3C). Moreover, cross-linking and gel filtration experiments did not show a significant trimer band or peak when we mixed Sav, Mst1, and Rassf5 SARAH domains together (SI Fig. 7). These results indicate that the mixture of the three different SARAH domains did not form a stable Sav·Rassf5·Mst1 ternary complex in the experimental condition.

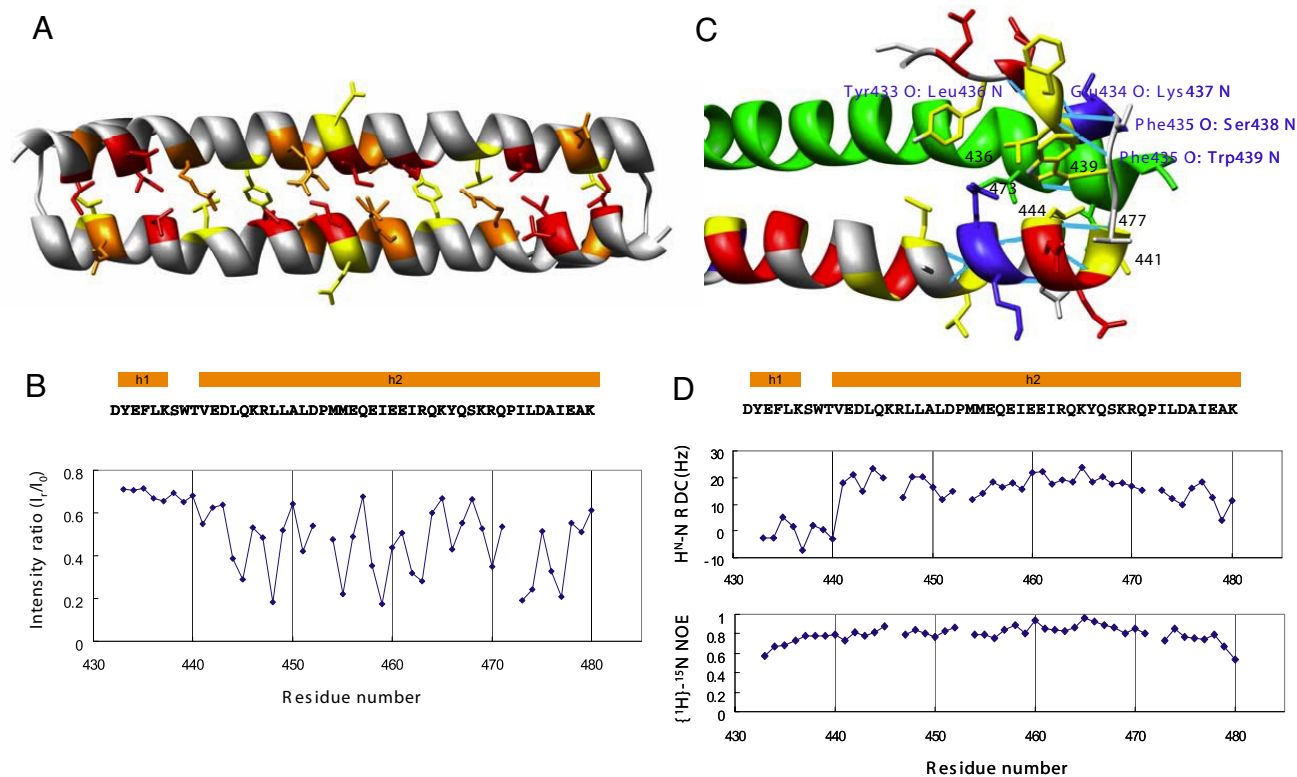


Fig. 2. Human Mst1 SARAH domain. (A) Ribbon representation depicting the side chains of residues having intermolecular interactions derived from the cross-saturation experiment (see *Materials and Methods*). Residues with intensity ratios <0.3 , $0.3-0.4$, and $0.4-0.5$ are red, orange, and yellow, respectively. (B) Plots of the intensity ratios of the cross-peaks in the cross-saturation experiments. The intensity ratios of the cross-peaks originating from the backbone amide groups with irradiation to those without irradiation are shown. The secondary structure elements, i.e., the 3_{10} helix h1 and the α -helix h2, are shown above the sequence. (C) Ribbon representation with the side chains of the N-terminal residues (432–451) showing the hydrogen bonding and hydrophobic interactions in this region. Hydrogen bonds are shown in cyan and labeled in blue, and the residues involved in hydrophobic interactions are labeled in black. Positively charged, negatively charged, and hydrophobic residues of the N-terminal part are blue, red, and yellow, respectively. The ribbon model of the other monomer is green. (D) Plots of the $^1\text{H}-^{15}\text{N}$ RDCs and heteronuclear $^1\text{H}-^{15}\text{N}$ NOE data of human Mst1 SARAH domain.

Disordered Structure of the Residues Linking the Kinase and SARAH Domains of Mst1. We expressed and purified the linker region between the kinase and SARAH domains of Mst1 (residues 326–401), which is also known as the inhibitory domain. By CD and one-dimensional NMR analysis (SI Fig. 8), we found that most of the residues in this region form a disordered structure, which can provide flexibility for domain motions in the Mst1 protein.

Discussion

Protein–protein interaction by SARAH domains plays a crucial role in apoptosis and cell cycle regulation through homodimerization as well as through heterodimerization with the RASSF tumor suppressor family (21). The structure of the human Mst1 SARAH homodimer shows unique structural features of the interactions mediated by the SARAH domain.

The SARAH homodimer of human Mst1 shows a novel structure in which the N-terminal 3_{10} helix is kinked from the main body. Helices h1 and h2 are connected by an extensive network of hydrophobic and hydrogen bonding interactions that are not only intramolecular but also intermolecular. The bifurcated hydrogen bonds from both Ser-438 and Trp-439 to Phe-435 are a unique feature for the stabilization of the conformation. We measured $^{15}\text{N}-^1\text{H}$ residual dipolar couplings (22) that are in agreement with the orientation of the N-terminal short helices h1/h1' in the SARAH homodimer, and we obtained mobility information from heteronuclear $^1\text{H}-^{15}\text{N}$ NOEs (23) that showed the substantial rigidity of the N-terminal short helix. Taken together, these findings are fully consistent with helix h1 stably

forming the kinked conformation against the long h2 helix that was observed in the solution structure.

Although the antiparallel helix conformation of the Mst1 SARAH domain shows some similarity with fragments of the ribosome recycling factor [Protein Data Bank (PDB) ID codes 1EK8 and 1DD5] or transmembrane proteins such as the F_1F_0 ATP synthase subunit c (1A91), they are not formed by self-association of two helices from different molecules. We could find a self-association example in the flock house virus B2 protein [2B9Z (ref. 24)], where the $\alpha 2$ - and $\alpha 2'$ -helices form an antiparallel homodimeric structure. However, helix h2 in the Mst1 SARAH domain is much longer (40 residues and 11 helical turns) than the $\alpha 2$ -helix of the flock house virus B2 protein (30 residues and 8 helical turns) and slightly bent because of the two proline residues (Pro-453 and Pro-472).

The analysis of cross-saturation between the two monomers further supports the dimeric structure seen in solution. The hydrophobic residues located at the dimer interface were affected by cross-saturation, which suggests that hydrophobic interactions are the main driving force for the dimerization. It was reported previously that mutation of Leu-444 disrupts dimerization (9). Leu-444 is a key structural residue in our homodimeric structure that contacts both helices and both monomers and is completely buried with $<1\%$ solvent-accessible surface area. Fifty-four NOEs (per monomer) originate from Leu-444, 22 of which are long-range, $|i - j| > 4$, and 17 are intermolecular. Obviously, a nonconservative mutation at this position can disrupt the dimer structure (see SI Fig. 9).

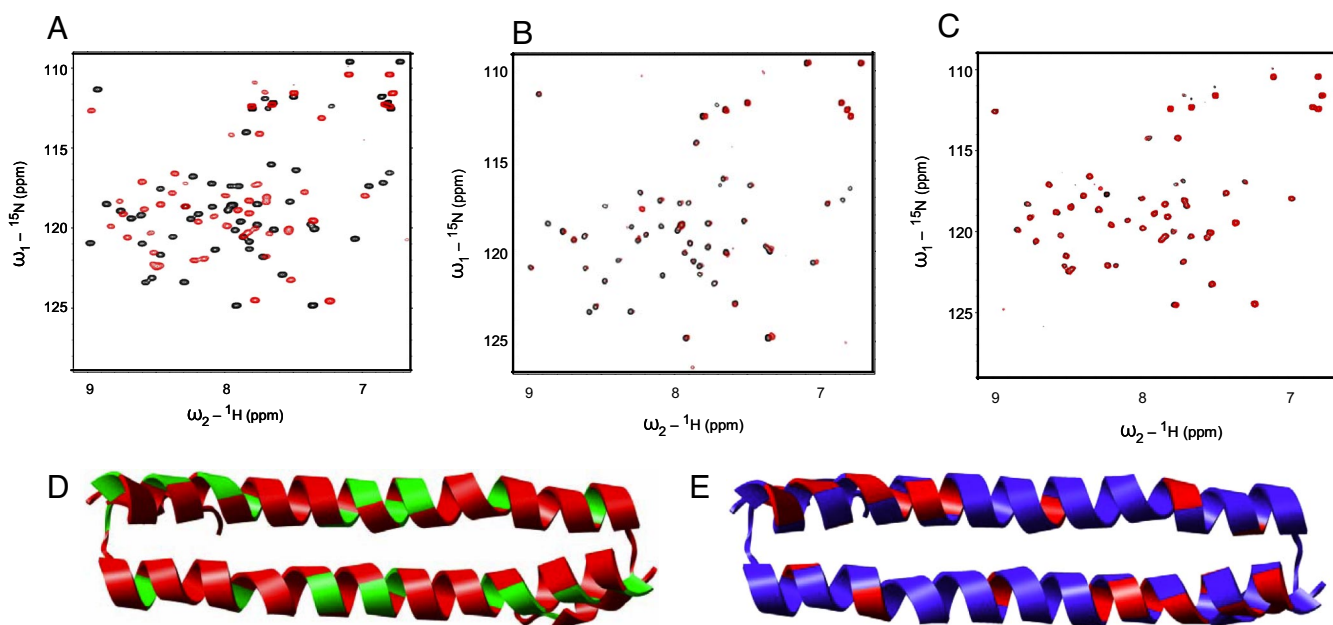


Fig. 3. Binding of the human Mst1 SARAH domain (432–480) to the human Rassf5 SARAH domain (220–270) and the human Sav SARAH domain (residues 321–373). (A–C) Chemical shift perturbations after the addition of 0.3 mM Rassf5 SARAH domain (A), 0.6 mM Sav SARAH domain (B), and 0.1 mM Rassf5 SARAH domain and 0.6 mM Sav SARAH domain (C) to 0.3 mM (A) and 0.1 mM (B and C) ^{15}N -labeled Mst1 SARAH dimer, respectively. The chemical shifts are monitored in ^1H , ^{15}N correlation spectra. The spectra of the free protein are shown in black, and the spectra after the addition of Rassf5 or Sav SARAH domain are shown in red (A and B). The spectra of a 1:1 mixture of the Mst1 and Rassf5 SARAH domain are shown in black, and the spectra after addition of Sav SARAH domain are shown in red (C). (D and E) Ribbon representation of the human Mst1 SARAH dimer colored according to chemical shift changes or broadening effects upon addition of the human Rassf5 SARAH domain (D) and Sav SARAH domain (E) (see A and B). In D, weighted average of the ^{15}N and ^1H chemical shift perturbations $\Delta\delta = (\delta\text{H}^2 + \delta\text{N}^2/5)^{1/2}$ of Mst1 SARAH domain on the addition of Rassf5 SARAH domain were calculated, and the residues with $\Delta\delta > 0.12$ ppm are colored red, other residues are green. In E, addition of the Sav SARAH domain to the Mst1 SARAH domain resulted in signal broadening for residues of the Mst1 SARAH domain. The residues with signal broadening, defined by peak intensities decreased to $<40\%$ of their original values, are colored red, other residues are blue. The same orientation as in Fig. 1A is shown.

Addition of the Rassf5 SARAH domain to the Mst1 SARAH domain resulted in a dramatic change of the NMR signals from the Mst1 SARAH domain, indicating that most residues of the Mst1 SARAH domain are affected by the heterodimerization. The chemical shift changes of the residues in the dimer interface are greater than those of the other residues located at the solvent-exposed side (Fig. 3D). This result implies that the heterodimeric formation involves the hydrophobic residues of the helical domain. The nearly 1:1 stoichiometry obtained from the titration experiment (Fig. 4A) shows that the affinity of heterodimer formation is stronger than that of the homodimer.

Interestingly, the appearance of additional signals near 8.5–9.0 ppm at ratios of Mst1 (0.3 mM) to Rassf5 (≥ 0.6 mM) of 1:2 and higher indicates that a further conformational change of the Mst1 SARAH domain was induced. A β -sheet structure may have been formed from the original helical structure. On the other hand, cross-linking experiments showed that significant structural changes of the Rassf5 SARAH domain occurred upon heterodimerization, as evidenced by the appearance of a strong dimer band and the concomitant disappearance of the tetramer band (Fig. 4B). Gel filtration chromatography gave a similar result, showing a shift of the retention time of the Rassf5 SARAH domain toward smaller size (SI Fig. 7B).

The broadening of Mst1 signals upon binding to Sav shows that the binding affinity of Sav to Mst1 is weaker than that of Rassf5 (Nore1) (25) and insufficient to dissociate the Mst1 SARAH homodimer. Moreover, most of the NMR signals affected are from hydrophilic surface residues (Fig. 3E), which differs from the case of Rassf5, where the signal changes occurred mainly at the dimer interface (Fig. 3D). Thus, the binding of the Sav SARAH domain to the Mst1 SARAH domain does not appear to interfere with Mst1 SARAH homodimerization.

As described in the binding study with the Sav SARAH domain, although Sav can bind to the Mst1 SARAH domain, it is not likely to form a stable Sav-Rassf5-Mst1 triple complex through the SARAH domains (Fig. 3C and SI Fig. 7A and B). From these observations, it is imaginable that MST plays dual roles to interact with different types of tumor suppressor in different stages of signaling. In the upstream branch of the MST signaling pathway, Mst1 forms a heterodimer with the Rassf1 or Rassf5 protein through SARAH domains, and in the downstream branch, Mst1 interacts with Sav through the SARAH domains to transfer the signal for apoptosis or cell cycle arrest. However, Mst1 may not bind simultaneously to both Rassf1/5 and Sav, at least not through the SARAH domains.

On the basis of the three-dimensional structure of the SARAH domain and the disordered nature of the linker region that connects it to the kinase domain, we can propose a model for the homotypic interaction of Mst1 and for its heterotypic interaction with RASSF family proteins (Fig. 5). Although the SARAH dimer comprises the antiparallel helix dimer structure of the h2 helices, the kinked short h1 helix in the N-terminal region of the SARAH domain enables the autophosphorylation of the kinase domain of Mst1. The linker region between the two domains is flexible also in the intact full-length Mst1, which makes it susceptible to cleavage during purification (data not shown). This feature might also be similar in the heterotypic interaction with RASSF family proteins that mediates the apoptosis signaling. The interaction between RASSF family tumor suppressors and MST kinases may induce the colocalization of the signal transduction machinery in the apoptosis pathway. The flexible nature of the linker region can facilitate dynamic conformational changes upon interaction between the SARAH domains of different classes of tumor suppressors.

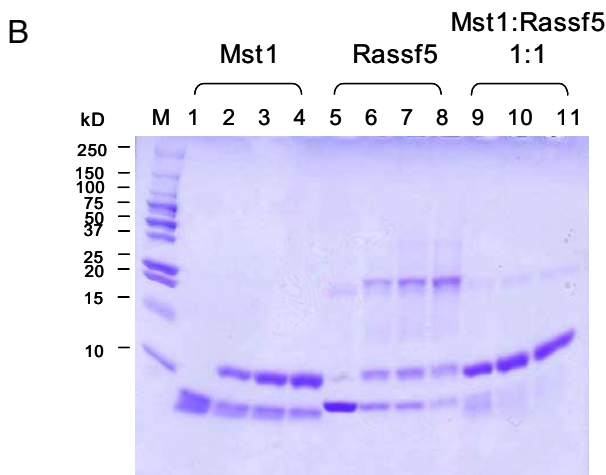
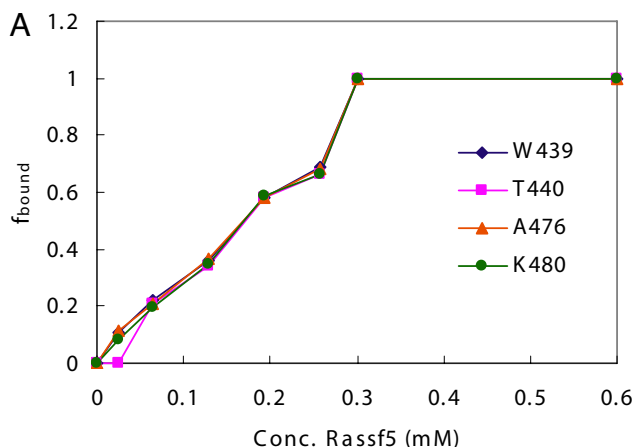


Fig. 4. Heterodimerization of Mst1 SARAH domain and Rassf5 SARAH domain. (A) Titration of the Mst1 SARAH domain with the Rassf5 SARAH domain. The fraction of bound protein (f_{bound}) is plotted as a function of the Rassf5 SARAH domain concentration. f_{bound} is defined in terms of the signal intensities by $f_{\text{bound}} = I_{\text{bound}} / (I_{\text{bound}} + I_{\text{free}})$, where I_{bound} and I_{free} are the peak intensities of the Rassf5 SARAH-bound and free NMR signals of the residues Trp-439, Thr-440, Ala-476, and Lys-480 of the Mst1 SARAH domain. The Mst1 SARAH concentration was 0.3 mM, and the Rassf5 SARAH concentrations were 0.03, 0.06, 0.13, 0.2, 0.26, 0.3, and 0.6 mM. (B) Cross-linking experiment of Mst1 and Rassf5 SARAH domains (see *Materials and Methods*). Lanes 1–4 are 0.1 mM Mst1 SARAH domain incubated with 0, 0.005, 0.01, and 0.02% (vol/vol) glutaraldehyde, respectively. Lanes 5–8 are 0.1 mM Rassf5 SARAH domain with 0, 0.005, 0.01, and 0.02% (vol/vol) glutaraldehyde, respectively. Lanes 9–11 are a 1:1 mixture of 0.1 mM Mst1 and Rassf5 SARAH domains incubated with 0.005, 0.01, and 0.02% (vol/vol) glutaraldehyde, respectively.

In summary, we described the structure of the human Mst1 SARAH domain and characterized its interaction with the Rassf5 SARAH domain. Our studies showed that the SARAH dimer adopts a novel fold including an antiparallel helix dimer structure. The combined structure analysis and binding study with Rassf5 provided the structural basis for the homo- and heterotypic interactions of the SARAH domain, which are crucial for apoptosis and cell cycle regulation.

Materials and Methods

Cloning, Expression, and Purification. The GST-fused human Mst1 SARAH domain (residues 432–480), human Rassf1c SARAH domain (residues 220–270), human Rassf5 (Nore1) SARAH domain (residues 366–413), and human Sav SARAH domain (residues 321–373) were synthesized by PCR. The products were digested with BamHI/XhoI and inserted into a pGEX4T-1

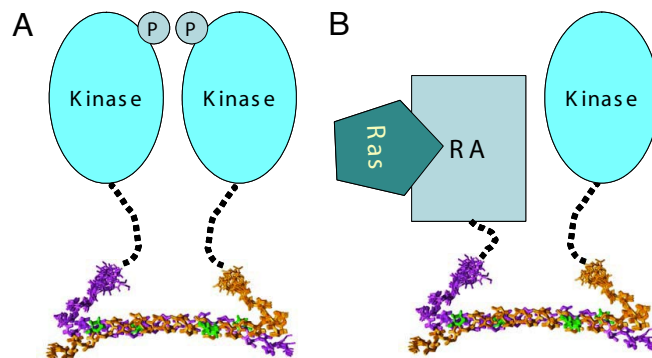


Fig. 5. Schematic model of the mode of homotypic interaction of Mst1 and heterotypic interaction with RASSF family proteins (See *Discussion*). (A) The Mst1 kinase domain is linked to the SARAH dimer through a flexible linker, which enables the kinase domain to perform autophosphorylation. (B) The Ras association domain of RASSF family tumor suppressors is linked to their SARAH domain, which mediates heterotypic interaction with Mst kinases. This interaction may induce the colocalization of the RASSF family tumor suppressors with MST kinases in the apoptosis pathway.

vector. The recombinant protein was expressed in *Escherichia coli* (BL21 strain) for 6 h at 25°C after induction by 1 mM isopropyl- β -D-thiogalactoside. For uniform labeling with ^{15}N , or with ^{15}N and ^{13}C , cells were grown in M9 minimal medium supplemented with $^{15}\text{NH}_4\text{Cl}$ without or with ^{13}C -labeled glucose, respectively. For the preparation of a ^2H , ^{13}C , ^{15}N -labeled sample, the cells were grown in minimal medium prepared with 100% D_2O . Cell lysates were purified by a GST column followed by gel filtration (Superdex-75 column) equilibrated with 25 mM Hepes/100 mM NaCl/2 mM DTT, pH 7.0. The Sav SARAH domain was not soluble when expressed in *E. coli*. The GST-fused Sav SARAH domain was extracted from cell pellets by agitation in 1.5% *N*-laurylsarcosine (sarkosyl)/2% Triton X-100. Extracted Sav was purified in the presence of 75 mM Hepes, pH 7.4/150 mM NaCl/5 mM DTT/0.1% Triton X-100, by using a GST column and gel filtration (Superdex-75 column).

The protein was concentrated to 0.2–1 mM for NMR experiments. For measurements in D_2O , the protein was lyophilized and redissolved in D_2O .

NMR Spectroscopy. NMR measurements were performed at 25°C on 1 mM ^{13}C , ^{15}N -labeled Mst1 SARAH domain samples in 25 mM Hepes, pH 7.0/100 mM NaCl/2 mM DTT/10% D_2O on Avance 500, Avance 800, and Avance II 900 spectrometers (Bruker, Rheinstetten, Baden-Württemberg, Germany). All NMR spectra were processed with NMRPipe and analyzed with SPARKY 3.110. ^1H , ^{15}N , and ^{13}C resonance assignments were obtained from the following three-dimensional heteronuclear correlation experiments: CBCA(CO)NH, CBCANH, HN(CA)CO, HNCO, HN(CO)CA, HNCA, HBHA(CO)NH, H(CCO)NH, C(CCO)NH, HCCH-COSY, CCH-TOCSY, and HCCH-TOCSY. Distance restraints were derived from ^{15}N - or ^{13}C -resolved three-dimensional NOESY. The intermolecular NOEs were detected by using a filter-edited three-dimensional NOESY spectrum. A ^{13}C , ^{15}N -labeled/unlabeled protein sample (1:2) was used for these experiments. Steady-state ^{15}N - ^1H NOEs of ^{13}C , ^{15}N -labeled Mst1 SARAH domain were measured following the methods described by Farrow *et al.* (23). ^1H - ^{15}N residual dipolar coupling constants were measured by using IPAP-HSQC experiments (22) in alignment medium with a stretched polyacrylamide gel. The cross-saturation experiments were performed by using the pulse scheme shown by Takahashi *et al.* (17). Measurements were made by using a sample of 1.0 mM ^2H , ^{15}N -labeled Mst1 SARAH domain in complex with 2.0

mM unlabeled Mst1 SARAH domain. For NMR titrations, 0.03, 0.06, 0.13, 0.2, 0.26, 0.3, 0.6, and 1.2 mM Rassf5 SARAH domain were added to a 0.3 mM solution of ^{15}N -labeled Mst1 SARAH domain up to a 4-fold molar excess. Chemical shifts were monitored in two-dimensional ^1H - ^{15}N HSQC experiments.

Structure Determination. Automated NOESY cross-peak assignments (26) and structure calculations with torsion angle dynamics (27) for the Mst1 SARAH homodimer were performed by using a modified version of the program CYANA 2.1 (unpublished data) that enables the use of RDC restraints, that takes the homodimer symmetry explicitly into account for the network anchoring of the NOE assignments (26), that ensures an identical conformation of the two monomers by imposing torsion angle difference restraints on all corresponding torsion angles, and that maintains a symmetric relative orientation of the two monomers by applying distance difference restraints between symmetry-related intermolecular C^α - C^α distances. For the use of RDCs, the alignment tensor magnitude of $D_a = 9.5$ Hz and rhombicity $R = 0.52$ were determined by using the program MODULE (28), based on the structures precalculated without RDC data. For residues located in regular secondary structure segments, ϕ and ψ backbone dihedral angle restraints were derived from chemical shifts by using the program TALOS (29). The 20 structures with lowest target function values were selected, and restrained energy minimization was performed with the program OPALp (30) by using the AMBER force field (31). The solution structure of the Mst1 SARAH domain was deposited in the Protein Data Bank (with PDB ID code 2J08).

Cross-Linking Experiments. These experiments are described in [SI Methods](#).

Structural Characterization of the Linker Region Between the SARAH and Kinase Domains. The linker region between the kinase and SARAH domain (residues 326–401) of human Mst1 was synthesized by PCR. The product was digested with BamHI/XhoI and inserted into a pGEX4T-1 vector. The recombinant protein was expressed in *E. coli* (BL21 strain) for 5 h at 37°C after induction by 1 mM isopropyl- β -D-thiogalactoside. Cell lysates were purified by a GST column followed by gel filtration (Superdex-75 column) equilibrated with 25 mM sodium phosphate/0.4 M NaCl/1 mM DTT, pH 6.0.

A one-dimensional ^1H NMR spectrum of the linker region construct was measured at 25°C by using 0.2 mM protein in 25 mM sodium phosphate, pH 6.0/0.4 M NaCl/1 mM DTT/10% D_2O on a Avance 500 spectrometer (Bruker).

CD measurements were performed at room temperature with a Jasco-715 spectropolarimeter by using a quartz cell with a path length of 1 mm. Far-UV CD spectra were monitored from 260 to 200 nm by using a protein concentration of 50 μM with 50 millidegree sensitivity, a response time of 1 s, and a scan speed of 20 nm/min. Spectra were recorded as an average of five scans. A background CD spectrum acquired from buffer was subtracted from the sample CD data.

Size-Exclusion Chromatography. Size-exclusion chromatography is discussed in [SI Methods](#).

This work was supported by funds from the 21C Frontier Functional Proteomics Project FPR 06B2-110 (to Y.H.J.) and by the Bio-MR Research Program E27070 (to Y.H.J., Korea Basic Science Institute) of the Korean Ministry of Science and Technology.

- Pantalacci S, Tapon N, Leopold P (2003) *Nat Cell Biol* 5:921–927.
- Harvey KF, Pflieger CM, Hariharan IK (2003) *Cell* 114:457–467.
- Wu S, Huang J, Dong J, Pan D (2003) *Cell* 114:445–456.
- Khokhlatchev A, Rabizadeh S, Xavier R, Nedwidek M, Chen T, Zhang XF, Seed B, Avruch J (2002) *Curr Biol* 12:253–265.
- Praskova M, Khokhlatchev A, Ortiz-Vega S, Avruch J (2004) *Biochem J* 381:453–462.
- Feig LA, Buchsbaum RJ (2002) *Curr Biol* 12:R259–R261.
- Scheel H, Hofmann K (2003) *Curr Biol* 13:899–900.
- Creasy CL, Chernoff J (1995) *J Biol Chem* 270:21695–21700.
- Creasy CL, Ambrose DM, Chernoff J (1996) *J Biol Chem* 271:21049–21053.
- Graves JD, Gotoh Y, Draves KE, Ambrose D, Han DK, Wright M, Chernoff J, Clark EA, Krebs EG (1998) *EMBO J* 17:2224–2234.
- Lee KK, Ohyama T, Yajima N, Tsubuki S, Yonehara S (2001) *J Biol Chem* 276:19276–19285.
- Graves JD, Draves KE, Gotoh Y, Krebs EG, Clark EA (2001) *J Biol Chem* 276:14909–14915.
- Lee KK, Murakawa M, Nishida E, Tsubuki S, Kawashima S, Sakamaki K, Yonehara S (1998) *Oncogene* 16:3029–3037.
- Ura S, Masuyama N, Graves JD, Gotoh Y (2001) *Proc Natl Acad Sci USA* 98:10148–10153.
- Cheung WL, Ajiro K, Samejima K, Kloc M, Cheung P, Mizzen CA, Beeser A, Etkin LD, Chernoff J, Earnshaw WC, Allis CD (2003) *Cell* 113:507–517.
- Oh HJ, Lee KK, Song SJ, Jin MS, Song MS, Lee JH, Im CR, Lee JO, Yonehara S, Lim DS (2006) *Cancer Res* 66:2562–2569.
- Takahashi H, Nakanishi T, Kami K, Arata Y, Shimada I (2000) *Nat Struct Biol* 7:220–223.
- Holm L, Sander C (1997) *Nucleic Acids Res* 25:231–234.
- Krissinel E, Henrick K (2004) *Acta Crystallogr D* 60:2256–2268.
- Callus BA, Verhagen AM, Vaux DL (2006) *FEBS J* 273:4264–4276.
- Agathangelou A, Cooper WN, Latif F (2005) *Cancer Res* 65:3497–3508.
- Cordier F, Dingley AJ, Grzesiek S (1999) *J Biomol NMR* 13:175–180.
- Farrow NA, Muhandiram R, Singer AU, Pascal SM, Kay CM, Gish G, Shoelson SE, Pawson T, Forman-Kay JD, Kay LE (1994) *Biochemistry* 33:5984–6003.
- Lingel A, Simon B, Izaurralde E, Sattler M (2005) *EMBO Rep* 6:1149–1155.
- Emerson SD, Madison VS, Palermo RE, Waugh DS, Scheffler JE, Tsao KL, Kiefer SE, Liu SP, Fry DC (1995) *Biochemistry* 34:6911–6918.
- Herrmann T, Güntert P, Wüthrich K (2002) *J Mol Biol* 319:209–227.
- Güntert P, Mumenthaler C, Wüthrich K (1997) *J Mol Biol* 273:283–298.
- Zweckstetter M, Bax A (2000) *J Am Chem Soc* 122:3791–3792.
- Cornilescu G, Delaglio F, Bax A (1999) *J Biomol NMR* 13:289–302.
- Koradi R, Billeter M, Güntert P (2000) *Comput Phys Commun* 124:139–147.
- Cornell WD, Cieplak P, Bayly CI, Gould IR, Merz KM, Ferguson DM, Spellmeyer DC, Fox T, Caldwell JW, Kollman PA (1995) *J Am Chem Soc* 117:5179–5197.